Optical and EUV Lithography

A Modeling Perspective

Andreas Erdmann

SPIE PRESS
Bellingham, Washington USA

Library of Congress Cataloguing-in-Publication Data

Names: Erdmann, Andreas, author.
Title: Optical and EUV lithography : a modeling perspective / Andreas Erdmann.
Description: Bellingham : SPIE–The International Society for Optical Engineering, 2021. | Includes bibliographical references and index.
Identifiers: LCCN 2020041503 (print) | LCCN 2020041504 (ebook) | ISBN 9781510639010 (paperback) | ISBN 9781510639027 (pdf)
Subjects: LCSH: Photolithography. | Extreme ultraviolet lithography.
Classification: LCC TR940 .E73 2021 (print) | LCC TR940 (ebook) | DDC 686.2/32–dc23
LC record available at https://lccn.loc.gov/2020041503
LC ebook record available at https://lccn.loc.gov/2020041504

Published by
SPIE
P.O. Box 10
Bellingham, Washington 98227-0010 USA
Phone: +1 360.676.3290
Fax: +1 360.647.1445
Email: books@spie.org
Web: http://spie.org

Copyright © 2021 Society of Photo-Optical Instrumentation Engineers (SPIE)

All rights reserved. No part of this publication may be reproduced or distributed in any form or by any means without written permission of the publisher.

The content of this book reflects the work and thought of the author. Every effort has been made to publish reliable and accurate information herein, but the publisher is not responsible for the validity of the information or for any outcomes resulting from reliance thereon.

Printed in the United States of America.
First Printing.
For updates to this book, visit http://spie.org and type "PM323" in the search field.

SPIE.

Contents

Preface *xiii*
Abbreviations and Acronyms *xvii*
Frequently Used Symbols *xxi*

1 Overview of Lithographic Processing **1**
1.1 From Miniaturization in Microelectronics Towards Nanotechnology 1
1.2 Historical Development 3
1.3 Aerial Image Formation in Projection Scanners 6
1.4 Photoresist Processing 10
1.5 Process Characteristics 13
1.6 Summary 19
References 20

2 Image Formation in Projection Lithography **23**
2.1 Projection Scanners 23
2.2 Theory of Image Formation 24
2.2.1 Fourier optical description 24
2.2.2 Oblique illumination and partially coherent imaging 30
2.2.3 Alternative image simulation methods 34
2.3 Abbe–Rayleigh Criteria and Consequences 35
2.3.1 Resolution limit and depth of focus 35
2.3.2 Consequences 40
2.4 Summary 44
References 45

3 Photoresists **47**
3.1 Overview, General Reaction Schemes, and Phenomenological Description 48
3.1.1 Classification of photoresists 48
3.1.2 Diazonaphthoquinone (DNQ)-based photoresists 51
3.1.3 State-of-the-art positive-tone chemically amplified resists (CARs) 53
3.1.4 Phenomenological model 54
3.2 Photoresist Processing Steps and Modeling Approaches 57
3.2.1 Selected technical aspects 57

3.2.2 Exposure 58
3.2.3 Post-exposure bake 62
3.2.3.1 Diazonapthoquinone (DNQ) resists 62
3.2.3.2 Chemically amplified resists (CARs) 64
3.2.4 Chemical development 66
3.3 General Remarks on Modeling Approaches and Compact Resist Models 70
3.4 Negative- versus Positive-Tone Materials and Processes 75
3.5 Summary 79
References 80

4 Optical Resolution Enhancements 87

4.1 Off-Axis Illumination 87
4.1.1 Optimum off-axis illumination for line-space patterns 89
4.1.2 Off-axis illumination for arrays of contact holes 90
4.1.3 From conventional and parametric source shapes to free-form illumination 92
4.2 Optical Proximity Correction 94
4.2.1 Compensation of the iso-dense bias 95
4.2.2 Compensation of line-end shortening 97
4.2.3 From rule-based to model-based OPC and inverse lithography 98
4.2.4 OPC models and process flows 101
4.3 Phase Shift Masks 103
4.3.1 Strong phase shift masks: Alternating PSMs 103
4.3.2 Attenuated or weak PSMs 110
4.4 Pupil Filters 113
4.5 Source and Mask Optimization 115
4.6 Multiple-Exposure Techniques 120
4.7 Summary 122
References 123

5 Material-Driven Resolution Enhancements 129

5.1 The Resolution Limit Revisited 129
5.2 Nonlinear Double-Exposure 133
5.2.1 Two-photon absorption materials 133
5.2.2 Optical threshold materials 134
5.2.3 Reversible contrast enhancement materials 135
5.3 Double and Multiple Patterning 137
5.3.1 Litho-etch-litho-etch (LELE) 137
5.3.2 Litho-freeze-litho-etch (LFLE) 138
5.3.3 Self-aligned double patterning (SADP) 139
5.3.4 Dual-tone development (DTD) 140
5.3.5 Selection of options for double and multiple patterning 141

5.4 Directed Self-Assembly (DSA) 142
5.5 Thin-Film-Imaging Technologies 148
5.6 Summary 149
References 150

6 Lithography with Extreme-Ultraviolet Light 157
6.1 Light Sources 159
6.2 Optical Material Properties in the EUV and Multilayer Coatings 161
6.3 Masks 164
6.4 Exposure Tools and Image Formation 169
6.5 Resists 173
6.6 Mask Defects 175
6.7 Optical Resolution Limits of EUV Lithography 179
6.7.1 Beyond EUV (BEUV) lithography at 6.*x* nm wavelength 180
6.7.2 Towards high-NA lithography 180
6.7.3 Towards smaller k_1: Optical resolution enhancements for EUV lithography 184
6.8 Summary 185
References 186

7 Optical Lithography Beyond Projection Imaging 197
7.1 Optical Lithography without a Projection Lens: Contact and Proximity Lithography 198
7.1.1 Image formation and resolution limit 198
7.1.2 Technical realization 201
7.1.3 Advanced mask aligner lithography 204
7.2 Optical Lithography without a Mask 209
7.2.1 Interference lithography 209
7.2.2 Laser direct write lithography (LDWL) 213
7.3 Optical Lithography without a Diffraction Limit 218
7.3.1 Near-field lithography 219
7.3.2 Employing optical nonlinearities 223
7.4 Optical Lithography in Three Dimensions 228
7.4.1 Grayscale lithography 229
7.4.2 3D interference lithography 231
7.4.3 Stereolithography and 3D microprinting 232
7.5 A Few Remarks on Lithography without Light 236
7.6 Summary 237
References 237

8 Lithographic Projection Systems: Advanced Topics 251
8.1 Wave Aberrations in Real Projection Systems 251
8.1.1 Zernike representation of wave aberrations 252

8.1.2 Wavefront tilt 256
8.1.3 Power aberration 257
8.1.4 Astigmatism 257
8.1.5 Coma 258
8.1.6 Spherical aberration 262
8.1.7 Trefoil aberration 263
8.1.8 Concluding remarks on Zernike-type wave aberrations 263
8.2 Flare 265
8.2.1 Constant flare model 266
8.2.2 Modeling of flare with power spectral densities 267
8.3 Polarization Effects in High-NA Projection Lithography 270
8.3.1 Mask polarization effects 270
8.3.2 Polarization effects in image formation 271
8.3.3 Polarization effects resulting from the resist and wafer stack interfaces 273
8.3.4 Polarization effects in the projector and the vector model for image formation 276
8.3.5 Polarized illumination 279
8.4 Other Imaging Effects in Projection Scanners 280
8.5 Summary 281
References 281

9 Mask and Wafer Topography Effects in Lithography 285
9.1 Methods for Rigorous Electromagnetic Field Simulation 287
9.1.1 Finite-difference time-domain (FDTD) method 289
9.1.2 Waveguide method 292
9.2 Mask Topography Effects 295
9.2.1 Mask diffraction analysis 296
9.2.2 Oblique incidence effects 299
9.2.3 Mask-induced imaging effects 300
9.2.4 Mask topography effects in EUV lithography and mitigation strategies 305
9.2.5 Variations of 3D mask models 310
9.3 Wafer Topography Effects 312
9.3.1 BARC deposition strategies 313
9.3.2 Resist footing close to poly-lines 315
9.3.3 Linewidth variation in double patterning 316
9.4 Summary 317
References 317

10 Stochastic Effects in Advanced Lithography 325
10.1 Random Variables and Processes 325
10.2 Phenomena 328

10.3 Modeling Approaches 332
10.4 Dependencies and Consequences 334
10.5 Summary 337
References 337

Index *343*

Preface

State-of-the-art semiconductor lithography combines the most advanced optical systems of our world with cleverly designed and highly optimized photochemical materials and processes to fabricate micro- and nanostructures that enable our modern information society. The unique combination of applied optics, chemistry, and material science provides an ideal playground for scientists and engineers with an interest in applied natural sciences and technology. For many years the development of lithographic patterning techniques was almost exclusively scaling driven and focused on the improvement of resolution to support Gordon Moore's vision of cramming more components onto integrated circuits. Although this scaling has still not reached its ultimate limits, it gets increasingly difficult and expensive to generate even more and smaller patterns on semiconductor chips with the required uniformity and without defects. Future lithographic techniques for emerging novel applications will have to emphasize different requirements, including three-dimensional (3D) shape control, integration of novel (functional) materials, patterning over non-planar surfaces, flexible adaptation of the target patterns to the final application, etc. The knowledge and experience of semiconductor lithographers, which were gained during more than 50 years of technology development, provide an important key to the development of novel micro- and nanotechnology-driven applications.

The material for this book was compiled over many years of giving lectures on Optical Lithography: Technology, Physical Effects, and Modeling at the Friedrich-Alexander-University Erlangen-Nuremberg and in preparation for dedicated courses on special aspects of lithography in companies and as side events of conferences. The book is intended to help interested students with backgrounds in physics, optics, computational engineering, mathematics, chemistry, material science, nanotechnology, and other areas to get started in the fascinating field of lithographic techniques for nanofabrication. It should also help senior engineers and managers to widen their view on alternative methods and applications.

It is not the intention of this book to provide a complete description of all aspects of lithographic patterning techniques. Instead, the book focuses on the explanation of the fundamental principles of image and pattern formation.

These fundamental principles are demonstrated by simple, hopefully easy to understand, examples. The pros and cons of certain approaches and technology options are discussed. Extensive lists of references direct the reader to articles and books for further reading on special topics. To limit both the volume of this book and the time needed to write it, several important aspects of lithographic patterning technologies are not or are only rarely addressed in this book: Metrology and process control becomes increasingly important for high-volume lithographic fabrication. Advanced DUV and EUV projection lithographies require flexible fabrication, inspection, tuning, and repair of high-quality masks. Modern semiconductor fabrication involves a close interaction between the designers of electronic circuits and lithography process technology experts to provide a lithography-friendly design. Finally, there are many non-optical lithography techniques. These aspects are covered in several other books and review articles.

There are already several excellent books on semiconductor lithography. Why do we need another book on this topic? Most importantly, because lithography is one of the most dynamic fields of technology. It evolves due to the integration of new ideas and technologies with very different backgrounds. Research and development for modern lithography is highly multidisciplinary. The precise fabrication and characterization of nanopatterns requires an in-depth understanding of all involved physical and chemical effects. This book tries to support such understanding from a modeling-driven perspective, but without relying on heavy mathematics. The contents of this book reflects my special interest and background in applied optics, diffractive optics, rigorous modeling, and optimization of the interaction of light with micro- and nanostructures. Consequently, mask- and wafer-topography effects and related light-scattering effects are more extensively discussed than in other books on lithography. Finally, this book aims to bridge the gap between highly specialized engineers in semiconductor fabrication and scientists and other engineers exploring novel applications of lithographic patterning techniques for alternative applications.

Optical (projection) lithography combines the imaging of a mask or template onto a photosensitive material (photoresist) with the processing of the photoresist to transfer the optical image into a 3D pattern. The first chapter of the book provides an introduction to aerial image formation and photoresist processing. Typical metrics for the quantitative evaluation of images, of photoresist profiles, and of lithographic process variations are explained. Analysis of these metrics helps one to understand the impact of image and process enhancements that are discussed in the following parts of the book.

Chapter 2 describes the image formation by superposition of diffracted light that is transmitted through the opening (numerical aperture) of a projection lens and focused onto the photoresist. The resolution limit of

projection systems is governed by the Abbe–Rayleigh equation. The fundamentals of photoresist chemistry and processing are explained in Chapter 3. The next two chapters provide an overview of resolution enhancements that are employed to print smaller features with a given wavelength and numerical aperture of the optical system. Optical resolution enhancements include off-axis illumination (OAI), optical proximity correction (OPC), phase shift mask (PSM), and source mask optimization (SMO). Multiple patterning and directed self-assembly (DSA) employ special materials and processing techniques to fabricate smaller features. Extreme-ultraviolet (EUV) lithography with a wavelength of 13.5 nm extends optical projection lithography into the spectral range of soft x-rays. There are no materials that transmit light at these small wavelengths. As explained in Chapter 6, EUV lithography has to employ reflective optics and mask, but also novel light sources and photoresist materials. Chapter 7 provides an overview of alternative optical lithography methods, including approaches to 3D lithography.

The remaining chapters of the book are dedicated to the description of important physical and chemical effects in advanced optical and EUV lithography. Chapter 8 discusses the impact of wave aberrations, polarization effects, and randomly scattered light on the intensity distribution inside the photoresist. Mask- and wafer-topography effects, which are caused by the scattering of light from small features on the mask and on the wafer, are described in Chapter 9. The last chapter of the book is devoted to stochastic effects that are responsible for non-smooth photoresist profiles with a line edge roughness (LER) on the order of a few nanometers and for the occurrence of fatal patterning defects such as microbridging and the incomplete opening of contact holes.

The order of the chapters follows the sequence of my lecture at the Friedrich-Alexander University Erlangen-Nuremberg. It is intended to provide an interesting mixture of theoretical background and application of optics and chemistry, and a description of various technology options. Chapters 1–5 describe the general background of optics and photoresist chemistry and should be read in this sequence. The reading order of Chapters 6–10 can be adapted to the special interests of the reader. Chapter 7 provides a general overview of alternative (optical) lithography methods that are more interesting for various applications of micro- and nanofabrication beyond nanoelectronics. People with exclusive interest in lithography for (advanced) semiconductor fabrication can skip this chapter.

Joint research work and fruitful discussions with many colleagues and project partners provided invaluable input for the material in this book. I am most grateful for suggestions from experts on special sections of this book, particularly the following: Antony Yen from ASML, Hans-Jürgen Stock from Synopsys, John Sturtevant from Mentor Graphics, Marcus Müller from the

University of Göttingen, Michael Mundt from Zeiss SMT, Uzodinma Okoroanyanwu from Enx Labs, and Raluca Tiron from CEA-Leti.

Many thanks to all present and former members and students of the Fraunhofer IISB Computational Lithography and Optics group, especially to Peter Evanschitzky, Zelalem Belete, Hazem Mesilhy, Sean D'Silva, Abdalaziz Awad, Tim Fühner, Alexandre Vial, Balint Meliorisz, Bernd Tollkühn, Christian Motzek, Daniela Matiut, David Reibold, Dongbo Xu, Feng Shao, Guiseppe Citarella, Przemislaw Michalak, Shijie Liu, Temitope Onanuga, Thomas Graf, Thomas Schnattinger, Viviana Agudelo Moreno, and Zhabis Rahimi. All of these people contributed to our Fraunhofer IISB Development and Research LiTHOgraphy simulator Dr.LiTHO, which was used to generate most of the figures in this book. Many useful remarks and tips from members of the Fraunhofer Lithography group and from students of my lithography lecture at the Erlangen University helped me to improve the material for this book.

Special thanks to Dara Burrows and Tim Lamkins from SPIE Press for their many useful tips and editorial assistance.

Andreas Erdmann
Erlangen, December 2020

Chapter 1
Overview of Lithographic Processing

This introductory chapter highlights the importance of lithographic processing techniques for the ongoing miniaturization of nanoelectronics and other emerging nanotechnologies. Lithography is used to fabricate increasingly smaller electronic and other devices with high accuracy and productivity. A short historical overview of the development of lithography in semiconductor fabrication is given. The fundamental components of projection systems for optical lithography and the basic steps in a lithographic process flow are introduced. This includes an overview of standard methods for the evaluation of projected images and resulting photoresist profiles. The chapter closes with an introduction of the most important methods for characterizing lithographic processes.

1.1 From Miniaturization in Microelectronics Towards Nanotechnology

The very first semiconductor amplifier, a point contact transistor, was developed by John Bardeen, Walter Brattain, and William Shockley at Bell Labs in 1947. They used two gold contacts held by a spring over a germanium crystal. The total size of this device was about 13 mm. Eleven years later in 1957, Jack Kilby at Texas instruments combined a silicon-based transistor, resistor, and capacitor to the first integrated circuit with a total size of 11 mm. It took more than another decade until a team lead by Federico Fedin, Ted Hoff, and Stan Mazor combined 2300 transistors to the first Intel 4004 microprocessor with a size of 4 mm. Since then, the number of transistors on semiconductor integrated circuits has grown enormously. The trend of this development is summarized on the left of Figure 1.1. Note the logarithmic scale of the vertical axis. This trend was already predicted in 1965 by Gordon Moore in his visionary article [1]. From today's perspective, Moore's prediction is interpreted as a doubling of the number of transistors every 18 months.

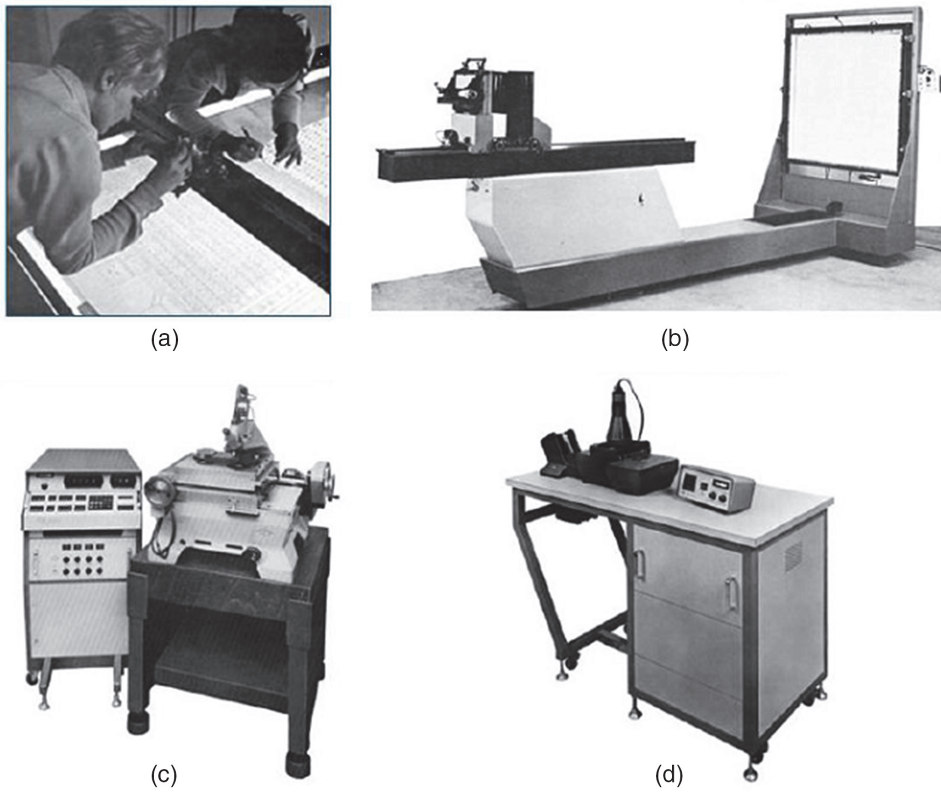

Figure 1.2 Lithographic pattern generation in the 1960s. (a) Manual inspection and repair of the Rubylith® master; (b) 10–50× reduction copy camera for fabrication of the reticle (photographic emulsion plate); (c) further 10× reduction for fabrication of the lithographic mask; (d) contact printer for exposure of the photoresist. Reprinted from Reference [6].

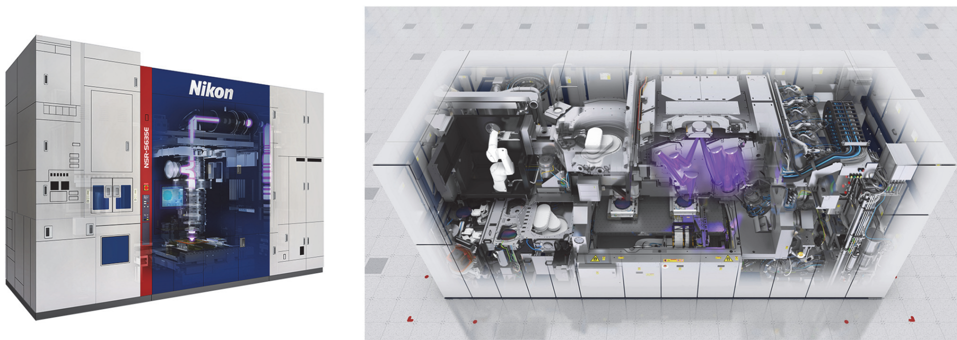

Figure 1.3 High-performance reduction scanners. Left: NSR-S635E NA = 1.35 immersion scanner of Nikon (courtesy of Donis Flagello / Nikon), operating wavelength 193 nm. Right: NXE-3400B EUV tool of ASML (courtesy of ASML), operating wavelength 13.5 nm.

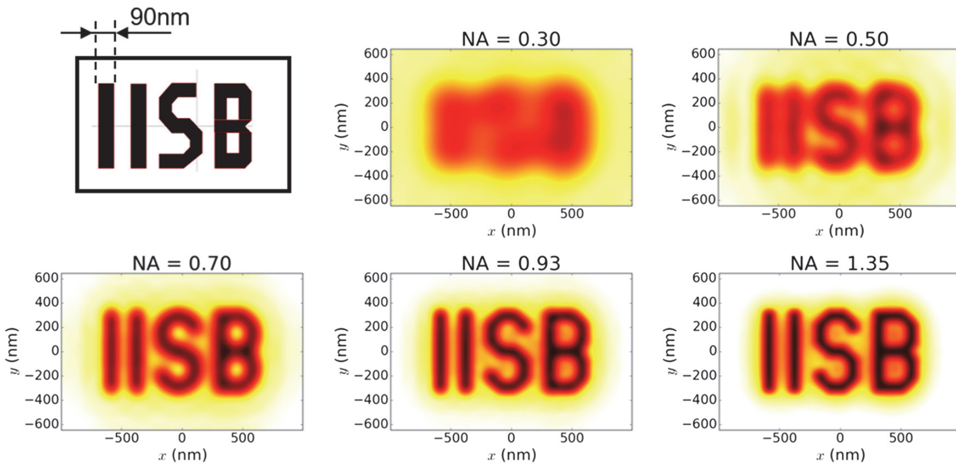

Figure 1.5 Image of a given mask layout (upper left) for different numerical apertures. The acronym IISB stands for Institut für Integrierte Systeme und Bauelementetechnologie, the German name of the Fraunhofer institute where the development and research lithography simulator Dr.LiTHO was developed. Dr.LiTHO is used for the majority of the presented simulations in this book. The width of the letter I in the mask layout is 90 nm. The images are computed for a wavelength of 193 nm.

Several methods have been developed to quantify the appropriateness of the obtained images for lithographic pattern transfer [8]. These methods are introduced in the remaining part of this section and in Section 1.5.

The simplest way to predict the shape of the printed feature on the wafer after the processing of the photoresist (see next section) is the application of a certain threshold. The footprint on the left of Figure 1.6 shows the result of

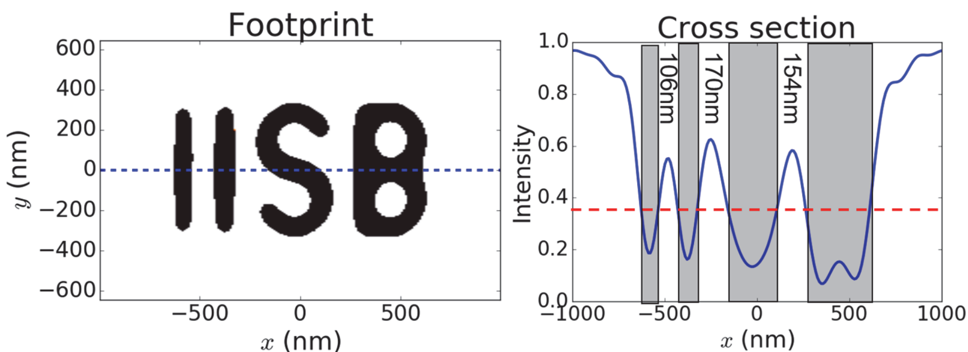

Figure 1.6 Application of a simple thresholding operation to the intensity distribution for an NA of 0.7 from Figure 1.5. Left: Footprint of the printed features for a threshold of 0.35. Right: Aerial image cross section at $y = 0$ and application of an intensity threshold at 0.35. The numbers at the top of the figure present the extracted feature sizes or critical dimensions (CD) of the corresponding bright features.

certain size of the process window. A larger process window suggests a more robust process. In the above examples, the Bossung curves and process windows are generated in terms of target sizes or CD data. In general, such process windows can also include other targets such as edge placements, feature positions, resist sidewall angles, and line edge roughness (LER).

Process linearity: Linearity curves such as those shown in Figure 1.15 characterize the scalability of the process. Bottom CDs of dense and isolated lines are computed versus the feature size. The dotted line in the figure indicates a perfectly linear process. For feature sizes above 150 nm both dense and isolated lines are very close to the ideal linearity curve. Features on the wafer are printed exactly as they are specified on the mask. Between 90 nm and 150 nm feature size there is a small difference in the slope of the curves. Dense and isolated features produce a slightly different CD. However, both curves are almost linear. Below 90 nm feature size the curves become increasingly nonlinear. The minimum CD for dense features is about 75 nm. This nonlinearity in the feature size transfer from mask to wafer has to be considered in the mask design (see Section 4.2).

Optical proximity effect (OPE) curves: Figure 1.16 presents simulated resist CD values of 90 nm lines versus period or pitch. The dose is chosen to print semi-dense lines with a pitch of 250 nm on target. The observed pronounced pitch dependency results from the impact of neighboring features on the resulting images or so-called optical proximity effects. Therefore, such curves are often called OPE curves. The shape of the OPE curve varies among different mask types, illumination geometries, and processing conditions.

Mask error enhancement factor (MEEF): The nonlinearities and proximity effects also have consequences for the fabrication tolerances of the masks [20]. The mask error enhancement factor (MEEF) is a measure of the sensitivity of the process to inaccuracies of the mask fabrication:

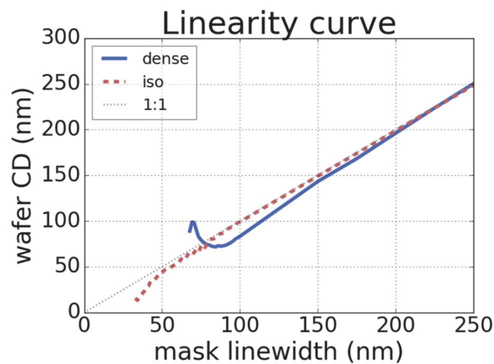

Figure 1.15 Simulated bottom CD of a resist for lithographic patterning of dense and isolated lines versus feature size. Imaging conditions: $\lambda = 193$ nm, NA $= 1.35$, circular illumination, resist thickness 150 nm.

Chapter 2
Image Formation in Projection Lithography

This chapter starts with a brief overview of the key performance parameters and features of modern deep-ultraviolet (DUV) projection scanners. The schematic presentation of a scanner optics from Section 1.3 is used to explain the theoretical background of image formation. Afterward, the Abbe–Rayleigh criteria for the resolution limits of optical projection lithography are derived and employed to discuss the general tendencies in the development of semiconductor lithography. A more detailed discussion of optical effects in real-world projection scanners is presented in Chapter 8.

2.1 Projection Scanners

Lithographic projection scanners are among the most advanced optical instruments. The basic principle of optical projection imaging was already introduced in Section 1.3. All lithographic projections scanners come with a high-NA projection lens and a flexible illuminator (condenser optics) to enable high-resolution imaging, mask- and wafer-stages to support high-throughput scanning exposures, and in-situ metrology to control the positions of the mask and wafer during the exposure. Typical technical specifications include the operating wavelength, e.g., 193 nm, a range of numerical apertures, e.g., 0.85–1.35, a single-exposure resolution, e.g., ≤38 nm, the maximum size of the image field, e.g., 26 × 33 mm, single-machine overlay, e.g., ≤1.4 nm, and production throughput, e.g., ≥275 wafers per hour. The example performance data are from the ASML TWINSCAN NTX:2000i system.

As indicated in Figure 1.4, both the condenser (illumination) and the projection system consist of many individual lenses. These sophisticated lens systems are designed using special optical ray tracing software [1]. The specifications of the design include a certain range of numerical apertures, a demagnification (typically 4×), and an image field size. Additional constraints

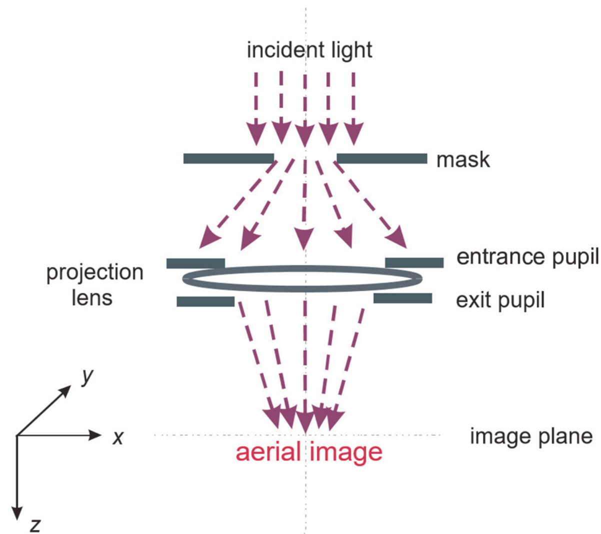

Figure 2.1 Schematic representation of coherent projection imaging.

the lateral coordinates x and y. Moreover, a paraxial propagation of the light in the system is assumed. The light is characterized by a scalar. No polarization effects are taken into account in this first simple approach to describe the image formation.

First, the light diffraction from the mask in the object plane x, y is computed (see Figure 2.2). The goal is to obtain the distribution of the light in the observation plane x', y' at a distance z from the object plane. The propagating light in the homogeneous region between the object and observation plane has to fulfill the scalar Helmholtz equation:

$$(\nabla^2 + \vec{k}^2)U = 0, \tag{2.1}$$

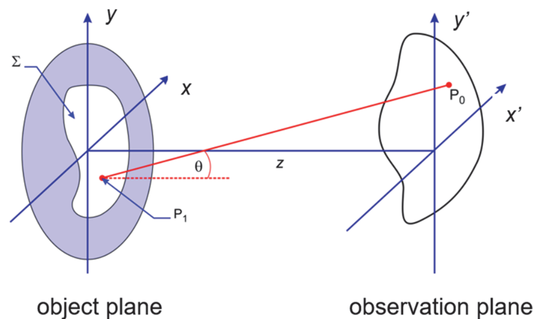

Figure 2.2 Diffraction problem: Incident light from the left is diffracted by an aperture in the object plane x, y. The diffracted light is detected in the observation plane x', y' at a distance z from the object plane. The intensity at the point P_0 in the observation plane is obtained as a superposition of light from all points P_1 inside the aperture Σ.

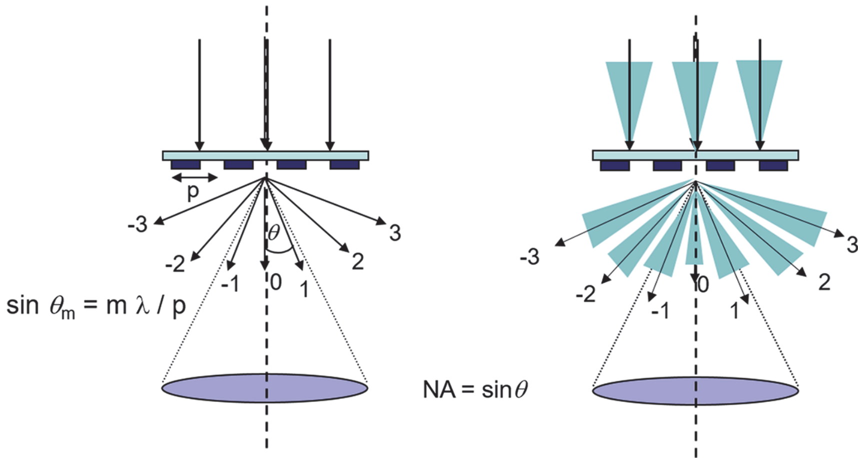

Figure 2.9 Coherent (left) and partially coherent (right) imaging. The arrows and cones indicate the directions of the illumination and of the diffracted light in the mth order (θ_m) for a mask with a line-space pattern and a pitch p. Redrawn from lecture material of Lawrence Berkeley National Laboratory, Center for X-ray Optics, 2005.

The image formation in partially coherent systems can be formulated by the Abbe method. The source is represented by discrete source points, which illuminate the mask with the angles θ_x^{inc}, θ_y^{inc}, and the corresponding spatial frequencies $f_x^{\mathrm{inc}} = \sin\theta_x^{\mathrm{inc}}/\lambda$, $f_y^{\mathrm{inc}} = \sin\theta_y^{\mathrm{inc}}/\lambda$, respectively. The complex amplitude of the scalar field at the image position is obtained by

$$a(x, y, f_x^{\mathrm{inc}}, f_y^{\mathrm{inc}}) = \mathfrak{F}^{-1}[P(f_x - f_x^{\mathrm{inc}}, f_y - f_y^{\mathrm{inc}})\mathfrak{F}(\tau(x, y))]. \tag{2.13}$$

In the above equation the shift invariance of the corresponding convolution operation has been used. The pupil function is shifted instead of the diffraction spectrum. Mathematically, this provides the same result.

Light that originates from different points of the source has no fixed phase relationship. Therefore, the resulting image for the complete source is obtained by the incoherent superposition of the images that are obtained for all discrete source points:

$$I(x, y) = \iint_{\mathrm{source}} a(x, y, f_x^{\mathrm{inc}}, f_y^{\mathrm{inc}}) \cdot a(x, y, f_x^{\mathrm{inc}}, f_y^{\mathrm{inc}})^* df_x^{\mathrm{inc}} df_y^{\mathrm{inc}}. \tag{2.14}$$

Figure 2.10 presents computed aerial images for different partial coherence factors σ. The image for fully coherent light ($\sigma = 0$) shows pronounced side-lobes. These are local minima and maxima in the vicinity of the main features. The usage of partially coherent light ($\sigma > 0$) reduces these sidelobes. Older generations of lithographic projection systems use partial

Chapter 3
Photoresists

Chapter 2 described the basics of aerial image formation. More advanced aspects of image formation, including wave aberrations, polarization effects in high-NA systems, and light scattering from topographic features on real masks and wafers, will be discussed in Chapters 8 and 9. The final goal of lithographic patterning, however, is to transfer these images or intensity distributions into micro- or nanostructures composed of distinct materials or into spatially modulated material properties. This is achieved by a light-induced modification of the solubility of a photoresist in combination with special processing techniques. The nonlinear behavior of photoresist enables the transfer of low-contrast and relatively smooth intensity distributions of images into binary profiles with nearly vertical edges.

The basic process flow for the resist patterning was already introduced in Section 1.4. This chapter provides an overview of typical photoresist materials and their modification during various processing steps. This includes the description of physical modeling approaches for the most important types of photoresist. These descriptions will be complemented by an overview of compact models for the photoresist that are used in many applications of computational lithography. The final part of this chapter will compare various aspects of negative- versus positive-tone photoresists and processes.

To enable a good transfer from (optically created) images to a patterned surface profile, the photoresist has to fulfill several requirements: First of all, the photoresist needs to have a sufficient resolution. This resolution or the achievable feature size can be potentially limited by diffusion of molecules, material inhomogeneities, mechanical stability, or other effects. To support a high throughput in semiconductor fabrication, short exposure times and high dose sensitivities of the photoresist are required. The photoresist has to be sufficiently transparent at the exposure wavelength. Otherwise, the bottom of the photoresist will not be exposed. On the other hand, a certain amount of light should be absorbed inside the photoresist to trigger chemical reactions that enable resist profile formation in the final development step. A good photoresist needs also to have a high contrast, i.e., a low sensitivity of the

Positive-tone resists become more soluble in the exposed areas. Negative-tone photoresists become less soluble in the exposed areas. During chemical development the parts of the resist with a higher solubility are washed away. The resulting photoresist profile serves as a template for other processing steps such as etching or doping.

A schematic comparison of a positive- and negative-tone photoresist process flow is given in Figure 3.1. In both cases the processing starts with a spin coating of the photoresist and a first baking step, frequently called the post-apply bake (PAB) or pre-bake. The exposure and the post-exposure bake (PEB) modify the solubility of the exposed photoresist areas. Depending on the tone, the chemical development washes away the exposed (positive tone) or unexposed (negative tone) parts of the photoresist. The remaining photoresist serves as a mask for selective etching of the underlying layer or other processing techniques like implantation, deposition, etc. Finally the photoresist is stripped off. The patterned layers that result from a positive- or negative-tone process are inverted relative to each other.

The solubility of photoresists in appropriate developer solutions can be modified by different mechanisms (see Reference [1], for example), as described below.

Change of polarity: The majority of the modern photoresist systems include a functional group that acts as a polarity switch. Diazonaphthoquinone (DNQ) photoresists, which are typically used in the spectral range between 350 nm and 450 nm, operate by a light-induced conversion of a base-

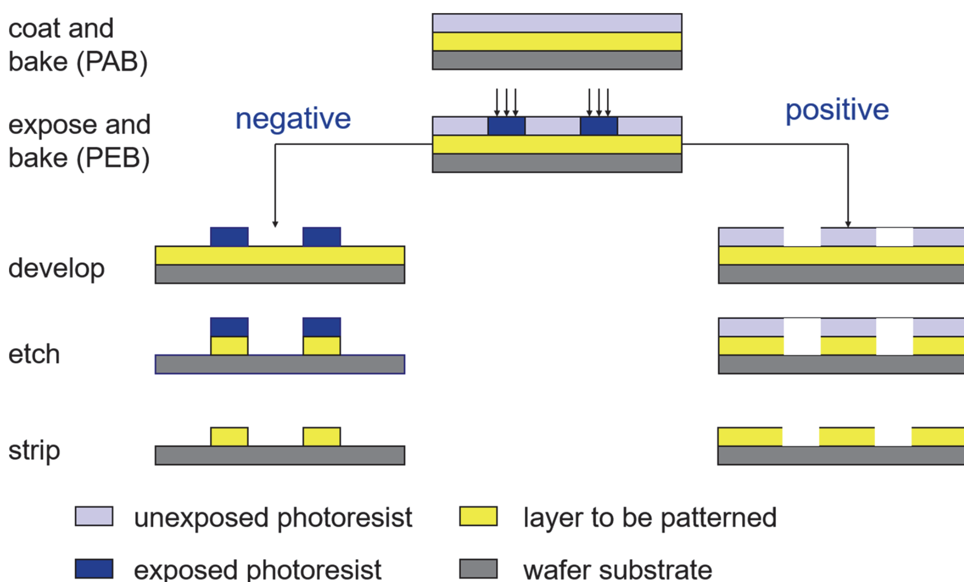

Figure 3.1 Schematic representation of positive- (left) and negative- (right) tone photolithographic processing.

curves are obtained by a series of uniform exposures — so-called flood exposures — of spin-coated resists with a defined thickness d_0 followed by a standard processing including chemical development. The thickness d of the remaining resist is measured for every exposure dose D. Figure 3.6 provides two representative examples of contrast curves of positive-tone resists. Here the remaining relative resist thickness d/d_0 is plotted versus the logarithm of the exposure dose D. The minimum dose value D_0, where the resist is completely removed ($d/d_0 = 0$) is called dose-to-clear. The photoresist contrast curve shows an almost linear behavior in a certain range below the dose-to-clear. Considering the logarithmic dose scale, this can be written as

$$\frac{d}{d_0} = \gamma \ln\left(\frac{D}{D_0}\right). \tag{3.1}$$

The photoresist contrast γ characterizes the steepness of the characteristic contrast curve close to the dose-to-clear. For dose values much smaller than the dose-to-clear, the relative thickness of both resists approaches 100%; i.e., the photoresist remains more or less unaffected by the exposure and further processing steps. The shown contrast curves differ in their steepness and corresponding values of γ. Some alternative definitions of the photoresist contrast and their pros and cons are discussed in Section 7.2 of Reference [20].

The photoresist is exposed with a spatially varying dose:

$$D(x, y) = t_{\text{exp}} I(x, y), \tag{3.2}$$

where t_{exp} is the exposure time and $I(x, y)$ represents the aerial image as obtained from the projection system. The exposure time is chosen in such way that the local dose $D(x, y)$ at the nominal edges of the target features is close to the dose-to-clear. Therefore, the sensitivity of the resist thickness d at the nominal feature edges is characterized by the linear part of the characteristic

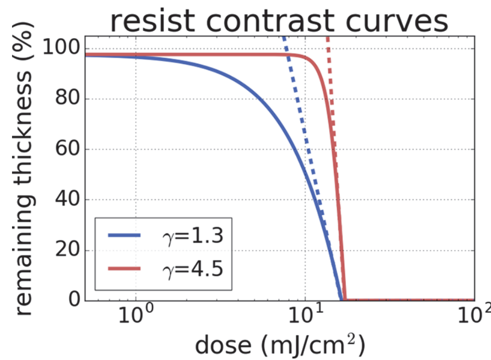

Figure 3.6 Characteristic contrast curves of a low-contrast (γ = 1.3) and a high-contrast (γ = 4.5) photoresist. The dashed lines indicate the linear slope of the contrast curve in a certain dose range below the dose-to-clear.

decrease the chemical contrast and reduce the process stability. Diffusion has no impact on the average amount of light intensity that is coupled into the resist, nor on the CD swings as shown in Figure 3.8.

3.2.3.2 Chemically amplified resists (CARs)

In contrast to DNQ-type resists, which are mainly characterized by the concentration of a single chemical species, the imaging mechanism of chemically amplified resists (CARs) involves several types of chemical species and corresponding reaction paths. The most important species and reactions are shown in Figure 3.10. As discussed in Section 3.1.3, the photosensitive species of CARs are photoacid generators (PAGs) that, when hit by a photon, release an acid A. This acid acts as a catalyzer for a chemical reaction that deprotects protected sides M. In addition, chemically amplified resists contain a certain amount of quencher base Q that reduces the amount of acid molecules that are available for the deprotection reaction.

The light-induced generation of photoacids happens already during the exposure. The fundamental imaging mechanism of a CAR involves an additional thermally driven or spontaneous deprotection reaction. In addition, several other reactions impact the photoresist perfomance. Most importantly, acids and quencher molecules that get close to each other will neutralize each other. Acids and quenchers can also get lost in other side-reactions or are driven out of the bulk resist. Moreover, heating the resist during the PEB can also cause deprotection reactions.

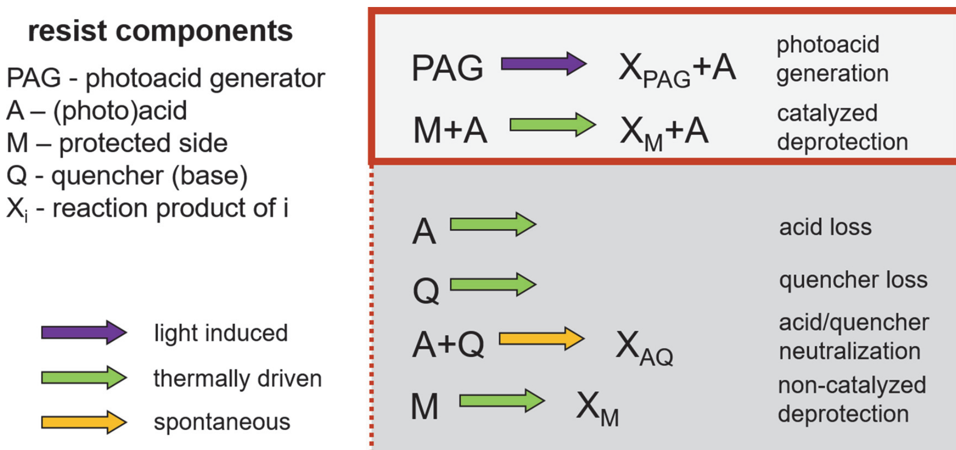

Figure 3.10 General reaction scheme of chemically amplified resists. The light-induced generation of photoacid and the acid-catalyzed deprotection in the upper right box are indispensable for the proper function of a CAR. The other reactions occur as well. The photoresist performance is also impacted by (thermally driven) diffusion of the acid and quencher.

Chapter 4
Optical Resolution Enhancements

This chapter presents methods to improve and optimize the image quality for systems with a fixed wavelength and a fixed numerical aperture. Optical resolution enhancements are applied in various parts of the lithographic system. Several examples from the previous chapter have already indicated the strong impact of the spatial coherence or the geometry of the illumination source on the image. The first section of this chapter explains how off-axis illumination is employed to improve the resolution and the quality of the obtained images. The next two sections describe important mask-related resolution enhancements. Optical proximity correction (OPC) modifies the geometrical shape of the absorber layout to compensate for image degradations that result from the diffraction limitation of the projection lens and from interactions between neighboring features on the mask. Phase shift masks (PSMs) utilize the phase of the light, which is transmitted by distinct areas of the mask, as an additional degree of freedom to achieve better images. The pros and cons of pupil filters in the projection lens are discussed in Section 4.4.

The two remaining sections of this chapter address two very important resolution enhancements. Source and mask optimization (SMO) applies various methods to identify the most appropriate source and mask geometries for the creation of given target patterns. Multiple-exposure techniques combine different sets of source and mask or focus settings to create images that cannot be obtained by a single exposure with a fixed source, mask, and focus setting.

4.1 Off-Axis Illumination

Figure 4.1 illustrates the basic principle of resolution enhancement by off-axis illumination (OAI). An incident plane wave is diffracted by a periodic mask pattern and generates several discrete diffraction orders. Only the 0th and $\pm 1^{st}$

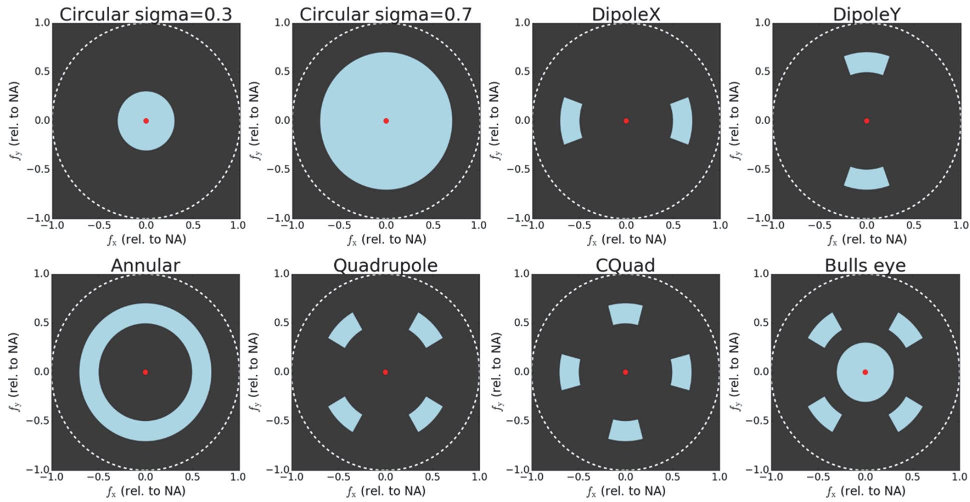

Figure 4.2 Typical standard illuminator shapes of projection scanners. The lighter-colored areas highlight the directions from which the mask is illuminated. These directions are specified with respect to the optical axis (small circle at the center of each box) and are scaled with the NA of the projection lens (dashed circle). Reproduced from Reference [1].

appropriate for imaging vertically (y-parallel) or horizontally (x-parallel) oriented line-space patterns. CQuad (CrossQuad) illumination provides the best illumination option for masks that include both vertical and horizontal lines. The annular illumination on the lower left is axial symmetric and does not introduce any orientation dependency. Quadrupole illumination, which is rotated 45 deg compared to the CQuad, provides the best illumination option for periodic and orthogonal arrays of square contact holes. The bull's eye on the lower right is a compromise for a combination of periodic and isolated features.

4.1.1 Optimum off-axis illumination for line-space patterns

What about the optimum illumination direction for specific mask features? Figure 4.3 demonstrates the application of a dipole to imaging a line-space pattern with period p. The diffraction angle $\theta_{\mathrm{out}}^{m}$ of the mth order of the

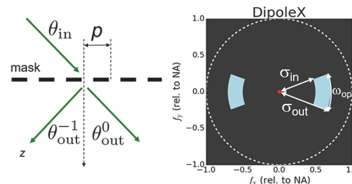

Figure 4.3 Dipole illumination for the imaging of lines and spaces with a period p. Side view of Littrow mounting (left) and top view of dipole configuration (right).

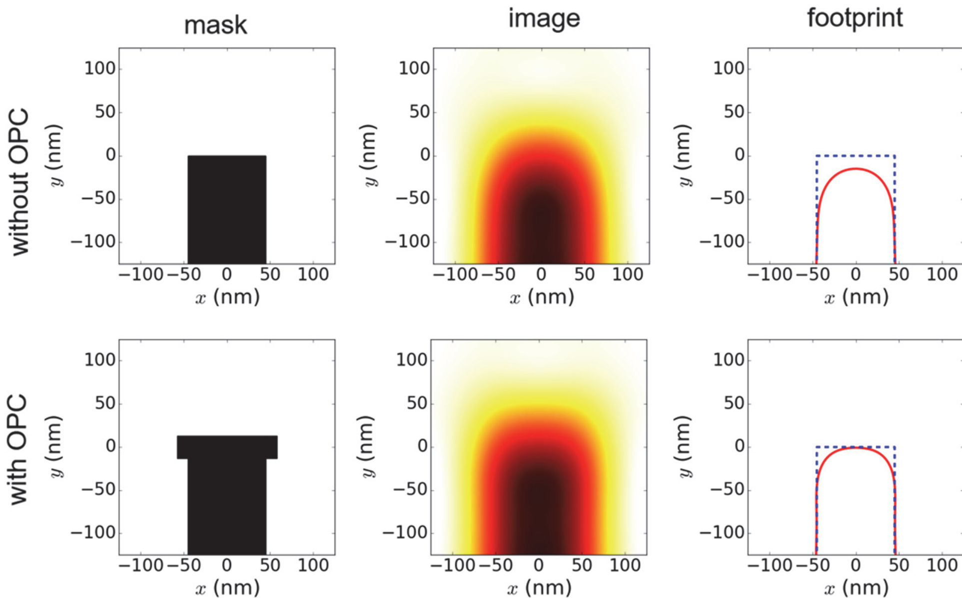

Figure 4.11 Simple OPC for line-ends. Mask layouts (left), aerial images (center), and comparison of simulated footprints (right, solid lines) and design target (right, dashed lines) of line-ends without (upper row) and with serifs (lower row). Simulation settings: 90 nm isolated lines, $\lambda = 193$ nm, CQuad illumination, NA = 1.35.

assist features close to the line-ends can provide additional improvement of the through-focus imaging of line-ends.

4.2.3 From rule-based to model-based OPC and inverse lithography

The observations on the impact of biasing, assists, serifs, and other mask corrections on lithographic imaging can be used to establish rules that are applied as corrections to the mask layout. A simple example is shown in Figure 4.12. If the target or design indent on the upper left is used as the mask, a photoresist footprint with significant deviations from the target is obtained (upper right). The ends of the resist footprint are pulled back compared to the target. Moreover, the profile shapes at the corners are strongly deformed. Several rule-based corrections are applied to obtain a new optical-proximity-corrected mask (OPC mask, lower right). The resulting footprint of the corrected mask is much closer to the target (lower right).

The application of a few rules to a given layout is straightforward. However, lithographic processing with decreasing technology factors k_1 produces more severe proximity effects. The interaction distances between different features grow compared to the feature size. More and more interaction scenarios have to be considered, and increasingly complex mask corrections are required to compensate for the proximity effects. The number of OPC rules increases exponentially. This makes purely rule-based OPC

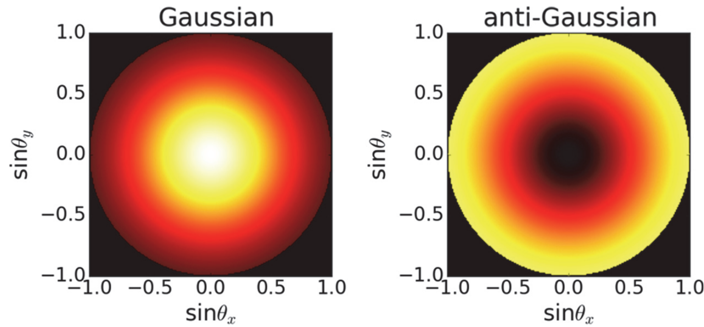

Figure 4.25 Examples of Gaussian (left) and anti-Gaussian (right) pupil transmission filters. The transmission varies continuously between low (dark) and high (bright) values.

imaging performance [41–43]. Figure 4.25 shows the transmission of Gaussian and anti-Gaussian filters. To simplify the discussion of the resulting imaging effects, a circular illumination shape with a small value of the partial coherence factor σ is considered here. In this case the Gaussian filter increases the weighting of low-spatial-frequency components that pass the center of the projection pupil, whereas the anti-Gaussian filter increases the high-spatial-frequency components close to the rim of the pupil.

Figure 4.26 presents simulated aerial image cross sections of 45-nm-wide isolated spaces without a pupil filter and with the shown Gaussian and anti-Gaussian filters. Both filters reduce the intensity of the transmitted light and the image intensity. The missing light is absorbed by the pupil filters inside the projection system. The resulting heating effects can cause uncontrollable wave aberrations and other distortions. Smith and Kang [44] propose the implementation of pupil filters on the mask pellicle, a thin protection layer separated from the mask pattern by about 6 mm.

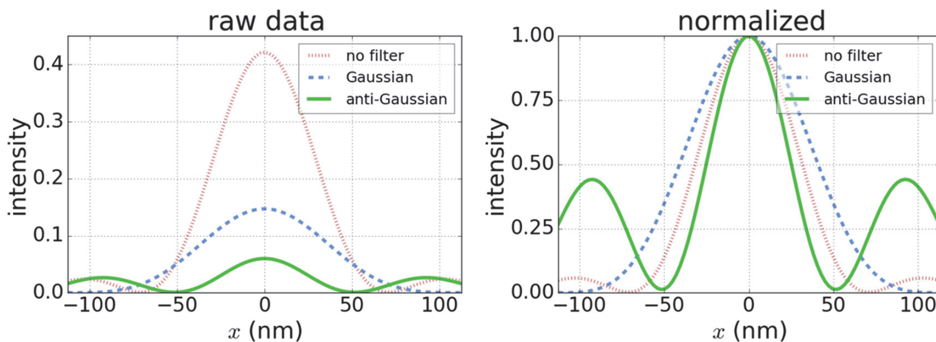

Figure 4.26 Aerial image cross sections of 45-nm-wide isolated spaces without and with Gaussian/anti-Gaussian–shaped pupil filters as shown in Figure 4.25. The raw data on the left are obtained with an open frame normalization. The data on the right are normalized to have a maximum intensity value of 1. Imaging conditions: $\lambda = 193$ nm, NA $= 1.35$, circular illumination $\sigma = 0.3$, best focus.

Chapter 5
Material-Driven Resolution Enhancements

Chapter 4 introduced important methods to enhance the resolution limits of lithography by modifying components of the optical imaging system, especially the mask and the illumination. These optical resolution enhancements aim to improve the image or intensity distribution that exposes the photoresist. This chapter presents important innovations that improve the pattern transfer of smaller features from given, diffraction-limited images into a spatial modulation of the photoresist or of other materials. The described techniques exploit specific (nonlinear) material properties and combinations of different materials and processing techniques. Therefore, we call them material-driven resolution enhancements.

This chapter starts with a brief review of some optical aspects of the resolution limit. A general patterning strategy is devised that enables the manufacturing of smaller patterns by appropriate superposition of multiple images and/or multiple process steps. The following sections introduce several specific double-exposure and double-patterning techniques that are used to push 193 nm immersion lithography to feature sizes below 45 nm. Directed self-assembly offers interesting options for a more-cost-effective scaling. The last section provides a brief overview of thin-film-imaging techniques that split the functionality of the photoresist into several materials and processes.

5.1 The Resolution Limit Revisited

The derivation of the resolution limit in Section 2.3.1 assumes a propagation and superposition of light in linear optical materials. The optical properties of these materials are independent from the intensity of the incident light. Nonlinear optical effects such as a light-induced modification of the extinction coefficient and/or refractive index can introduce several effects that do not follow the Abbe–Rayleigh criteria. An optical material that exhibits an increased refractive index in the exposed regions can act as a focusing lens and

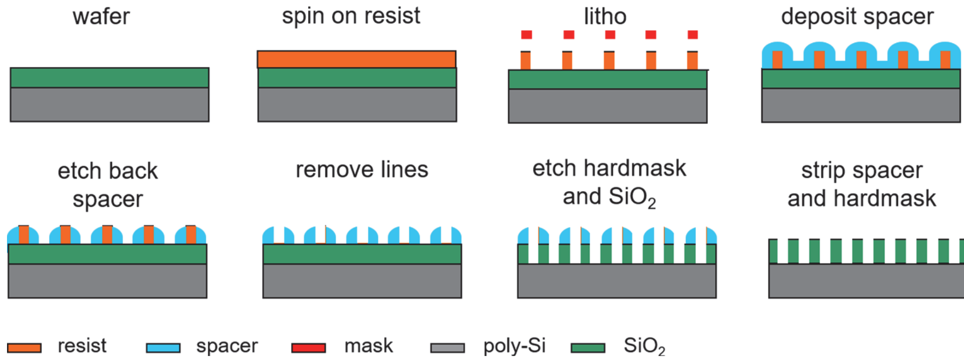

Figure 5.10 Self-aligned double-patterning (SADP) processing sequence. Sometimes this processing technique is also referred as spacer-defined double patterning (SDDP).

and to the right of each resist line. First, a standard lithography process is used to create semi-dense lines. Then, a spacer material (for example, Si_3N_4) is conformly deposited on the top of the patterned photoresist by a process such as chemical vapor deposition (CVD). Next, the spacer material is anisotropically etched and is therefore completely removed everywhere except along the sidewalls of the patterned sacrificial material. Finally, the resist is selectively removed, and the substrate can be etched using the remaining spacers as a masking layer [26,27].

SADP involves only a single lithography step. It does not suffer from overlay errors between two lithography steps. However, the distance between the spacers is very sensitive to CD and sidewall non-uniformities of the lithographically created sacrificial features, referred to as mandrels. Variation of the mandrel CD will cause the pitch between features to alternate, a phenomenon known as pitch walking [28].

The processing sequence from Figure 5.10 can be applied to other geometrical shapes of the sacrificial features as well. The creation of spacers along the sidewalls of lithographically created mandrel features and the selective removal of spacers at certain locations by trim exposures offer a certain design flexibility [27]. The application of two subsequent SADP process flows enables a further reduction of the pitch. The spacers from the first SADP become mandrels for the second SADP flow in self-aligned quadruple patterning (SAQP).

5.3.4 Dual-tone development (DTD)

Dual-tone development (DTD) was first proposed by Asano [29]. DTD achieves a pitch that is two times smaller by performing two separate development steps to remove the photoresist in the regions with the highest and lowest exposure doses. The basic principle of DTD is demonstrated in Figure 5.11. The resist is exposed with a line-space pattern. The resulting acid

Chapter 7
Optical Lithography Beyond Projection Imaging

This chapter provides an overview of diverse alternative optical lithography techniques that do not employ projection imaging of a mask. People with exclusive interest in projection lithography for semiconductor lithography can skip this chapter. For others it provides an overview of alternative optical lithography methods for alternative applications, including a more in-depth discussion of the optical nonlinearities that were already briefly addressed in Section 5.2.

Mask proximity printing is done without an (expensive) projection lens. Although this limits the achievable resolution and process control, it offers a cost-effective solution for less-demanding applications. Laser direct write and interference lithography provide options for pattern generation without a mask. Special optical near-field techniques and optical nonlinearities promise resolution capabilities that are not limited by diffraction.

Although these techniques do not simultaneously provide the high throughput, resolution, flexibility, and/or process control of DUV and EUV projection lithography, they find interesting applications in many areas of micro- and nanofabrication. The economical and technical investment in these techniques is more affordable for research institutes and small- or medium-size companies. The described methods can address special requirements that are not the focus of state-of-the-art semiconductor lithography, including very flexible patterning of low numbers of wafers, realization of special 3D profile shapes, application of non-standard materials, patterning over large areas, extreme wafer-topography or flexible substrates, etc.

The last section provides a brief description of e-beam and nano-imprint as the main representatives of non-optical lithography techniques.

The goal of this chapter is to introduce the fundamental concepts of these alternative optical lithography methods and to explain their advantages and disadvantages. Some of the described approaches are already being used in commercial solutions. Other concepts are only available as “home-made”

Chapter 8
Lithographic Projection Systems: Advanced Topics

In Chapter 2 we used several simplifying assumptions to discuss the image formation in an idealized projection imaging system. The projection optics was diffraction limited, i.e., without optical aberrations, randomly scattered light, or flare. The mask and wafer were placed at fixed and ideal positions in the object and image plane, respectively. Monochromatic light with an infinitely small bandwidth and a perfect illumination system were employed. Moreover, all polarization effects were neglected. The electromagnetic fields and the transfer functions of the system were treated as scalars. In this chapter we will discuss physical effects that occur in real-world projection systems that do not fulfill the simplifying assumptions noted above.

We start with a discussion of optical wavefronts in real projection systems. A Zernike representation of these wavefronts is used for the quantitative analysis of the relevant phenomena. The impact of specific Zernike wave aberrations (such as spherical aberration, astigmatism, and coma) on the lithographic imaging of typical mask patterns will be investigated. The second section provides a brief introduction to flare or randomly scattered light. Various polarization effects that occur in high-NA projection systems are described in Section 8.3. Specifically, the role of polarization in image formation and thin film interference effects will be discussed. The last section of this chapter provides a short discussion of image blur effects resulting from mechanical vibrations and from the finite bandwidth of the excimer lasers being used.

8.1 Wave Aberrations in Real Projection Systems

As described in Chapter 2, an ideal diffraction-limited projection system transfers a diverging spherical wave emerging from a point in the object plane into a part of a spherical wave that converges towards the image plane (see Figure 2.5). The wavefront transformation from the entrance to the exit pupil of

Andreas Erdmann is the head of the Fraunhofer IISB Computational Lithography and Optics group and teaches as “Privatdozent” at the University of Erlangen. He has more than 25 years of experience in optical and EUV lithography. He chaired SPIE conferences on Optical Microlithography and Optical Design, and is an organizer of the International Fraunhofer Lithography Simulation Workshop. He contributed to the development of several advanced lithography simulators, including the development and research lithography simulator Dr.LiTHO. He is Fellow of SPIE.